# Holdup Measurements on an SRNL Mossbauer Spectroscopy Instrument

**R. A. Dewberry, T. B. Brown, and S. R. Salaymeh**
**Savannah River National Laboratory**
**Aiken, SC 29808**
**USA**

## Abstract
Gamma-ray holdup measurements of a Mossbauer spectroscopy instrument are described and modeled. In the qualitative acquisitions obtained in a low background area of Savannah River National Laboratory, only Am-241 and Np-237 activity were observed. The Am-241 was known to be the instrumental activation source, while the Np-237 is clearly observed as a source of contamination internal to the instrument. The two sources of activity are modeled separately in two acquisition configurations using two separate modeling tools. The results agree well, demonstrating a content of (1980±150) μCi Am-241 and (110±50) μCi of Np-237.

## INTRODUCTION
The Savannah River National Laboratory (SRNL) has retired a Mossbauer spectroscopy instrument from one of its laboratory modules and required a measure of radioactivity content for disposition. While active, the instrument contained a 5mCi Am-241 solid activation source, and the facility radiation control group observed unknown contamination near the instrument base. The SRNL Analytical Development (AD) field nuclear measurement group was requested to identify the source of contamination near the instrument base and to evaluate its content.

The AD field measurement group has extensive experience using the Ametek ISOTOPIC software program to make the determination required.[1-3] The program is very useful for performing geometry corrections to transform point source calibration data into finite geometry source activity and to perform sample and container photon absorption corrections also. In the benchmark paper of reference 3, the AD group demonstrates the ISOTOPIC program's extensive utility with multiple radionuclides in diverse process holdup configurations and waste containers.

For holdup in the Mossbauer instrument the authors recognized a good opportunity to obtain a comparison of the ISOTOPIC analysis technique with the GADRAS analysis technique.[4] The GADRAS technique is used in nonproliferation γ-ray measurements and by the Department of Homeland Security Reach-back groups at SRNL. Our comparison should make an important contribution toward establishing the firm credibility of both measurement and evaluation techniques.

## EXPERIMENTAL

Photographs of the Mossbauer instrument and the two separate acquisition configurations are shown in Figures 1 and 2. The Mossbauer instrument is approximately cylindrically shaped with an outside diameter of nine inches and an overall height of 48 inches. The cylindrical container wall thickness is 0.2 inch stainless steel, and the container wall thickness at the bottom is 0.1 inch of stainless steel. The acquisition of Figure 1 shows the instrument being assayed through the cylindrical wall with a 20% high purity germanium (HpGe) detector at a detector standoff of 50 inches. The acquisition of Figure 2 shows the instrument being assayed through the 0.1 inch base at a detector standoff of 36 inches.

A Radiation Control (RCO) survey indicated contamination on the inside bottom to a height of approximately six inches. We used this as guidance for subsequent modeling of the activity observed. We were aware that the instrument contained a shielded Am-241 excitation source of approximately 5 mCi activity. The source of contamination was unknown, and the γ-ray acquisitions were required for both qualitative and quantitative determination. Since the two sources had different geometry, the quantitative assay presented a very interesting modeling problem that we describe in this paper.

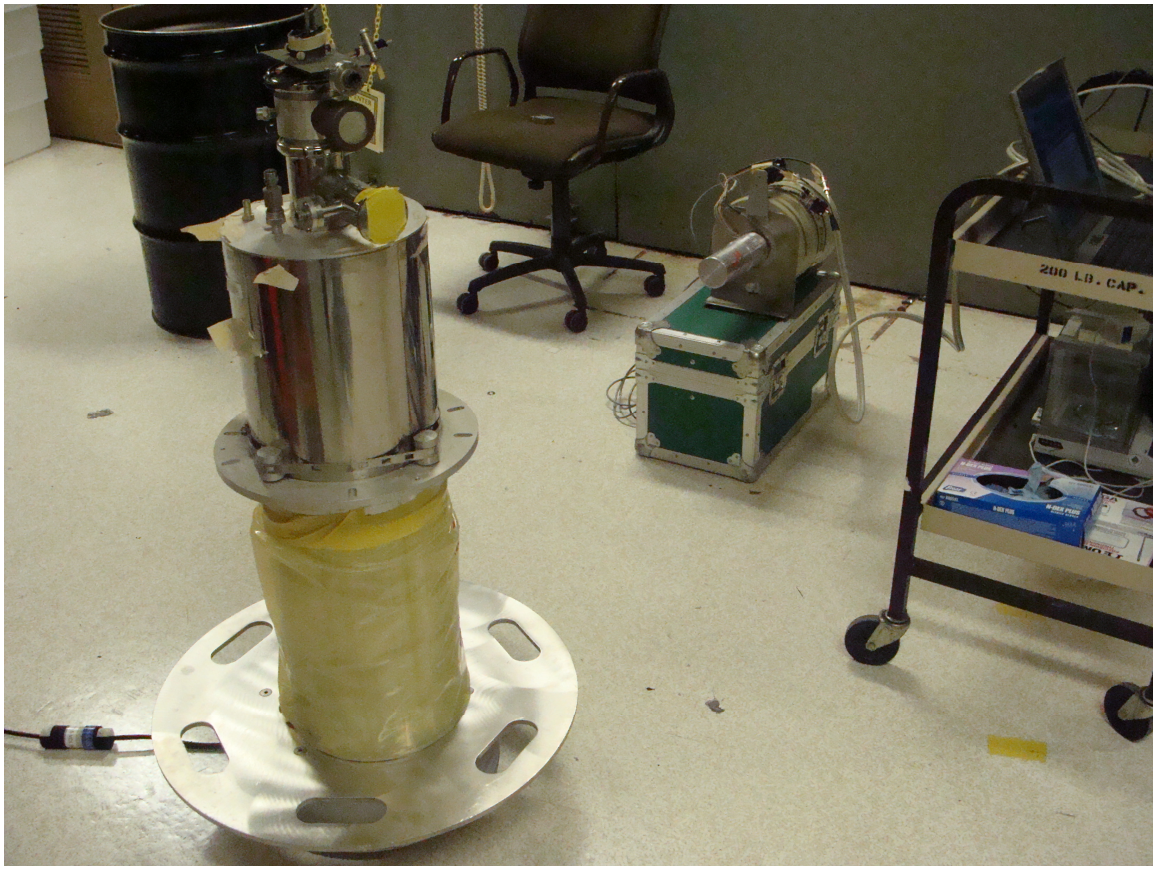


**Figure 1. A radial acquisition of the instrument's cylindrical base.**

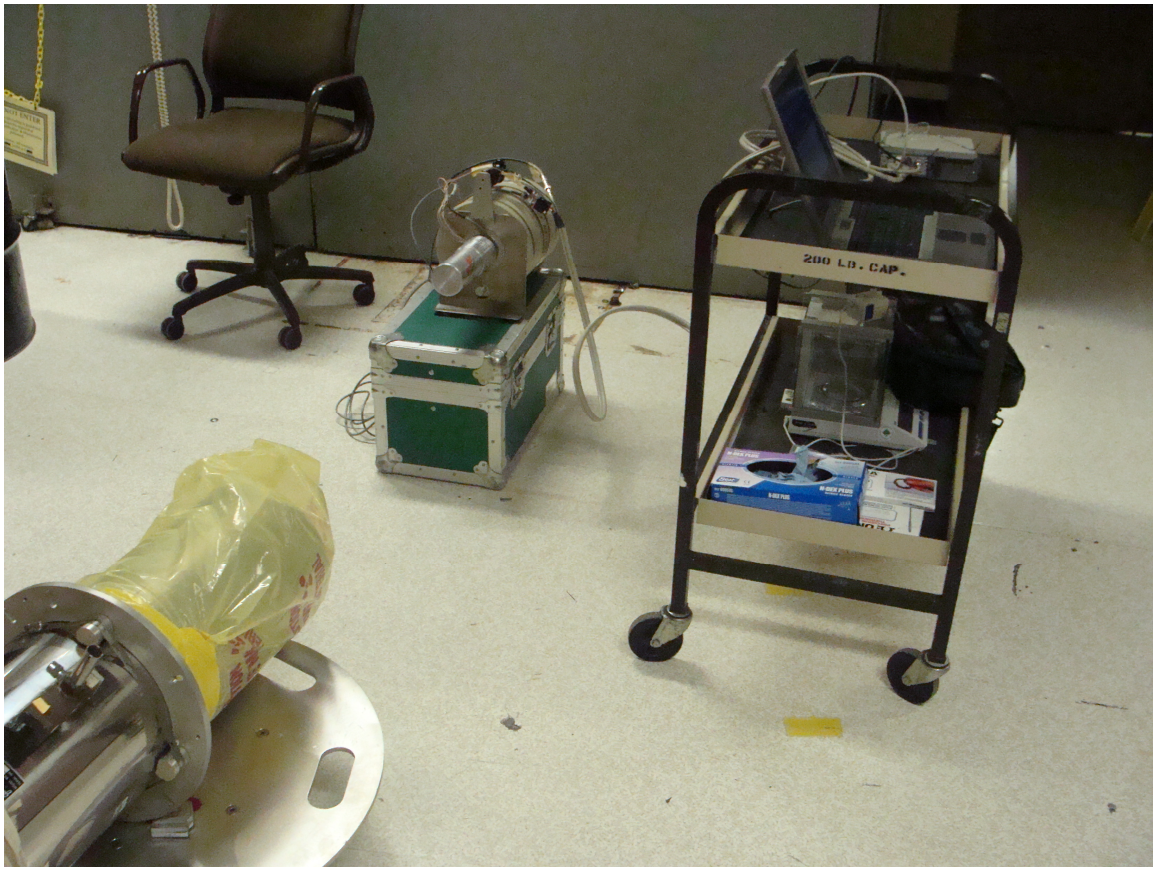


**Figure 2. An axial acquisition of the instrument's cylindrical base.**

To conduct the γ-ray acquisitions to evaluate the instrument, we moved it to a low background region of SRNL. In this area we were adjacent to the Solid Waste Assay Facility of SRNL, and we observed minor contributions from Am-241, Pu-239, and Cs-137 in the one-hour background. Other naturally occurring radioactivity and K-40 also appeared. The initial γ-ray spectrum acquired in the cylindrical configuration at a distance of 50 inches is shown in Figure 3, and the axial acquisition spectrum from 36 inches is shown in Figure 4. The data acquired are summarized in Table 1.

**Table 1. Detected event rates for selected photons in each acquisition configuration.**

| Acquisition | 60 keV (cps) | 312 keV (cps) | 300 keV (cps) | Live Time (sec) |
|---|---|---|---|---|
| *Axial 36* | **304.48** | **106.71** | **17.82** | **136.51** |
| *Axial 72* | **84.30** | **30.18** | **5.238** | **703.59** |
| *Radial 25* | **Not observable** | **41.16** | **6.694** | **3600** |
| *Radial 50* | **Not observable** | **15.64** | **2.679** | **3600** |

Note in the radial view, where the photons must pass 0.2 inches of steel, the Am-241 60-keV peak and the Np-237 and Am-241 decay x-rays at 86-keV and 99-keV are strongly attenuated relative to the 312-keV γ-ray from Np-237 decay. In the axial view, where the Np decay x-rays are passing through only 0.1 inch of steel, they appear much

stronger relative to the 312-keV γ-ray. The Am-241 decay photons at 60-keV, 94-keV, and 99-keV are passing through no instrument attenuation as there is a hole in the bottom that allows the detector a completely unobstructed point source view of the Am-241 activation source. These characteristics contributed to the interesting modeling problem.

The data were modeled with both the ISOTOPIC analysis program[1] and the GADRAS (Gamma Detector Response Analysis Software) analysis program[4]. We have used the former extensively to model holdup contamination in three drum repackage gloveboxes[2] and have benchmarked its capabilities against extensive tests in multiple acquisition configurations and against the GADRAS, Canberra ISOCS, and Microshield photon transport and analysis codes.[3,5] The GADRAS analysis technique uses previous detector characterization to fit an entire spectrum including the Compton continuum to estimate the contribution from single or multiple sources. With GADRAS we are able to fit γ-ray photopeaks plus the Compton Scatter continuum to determine contributions from selected species and to evaluate shielding.

Like GADRAS, ISOTOPIC requires previous detector calibration. In the acquisitions described we used a 20% relative efficiency HpGe detector that had been previously efficiency calibrated in point source configuration using a reference Ho-166$^{m}$ source at a distance of twelve inches. ISOTOPIC is able to calculate sample and container energy-dependent absorption factors and geometry correction factors to transform the 12-inch point source calibration curve to a finite geometry real acquisition configuration.

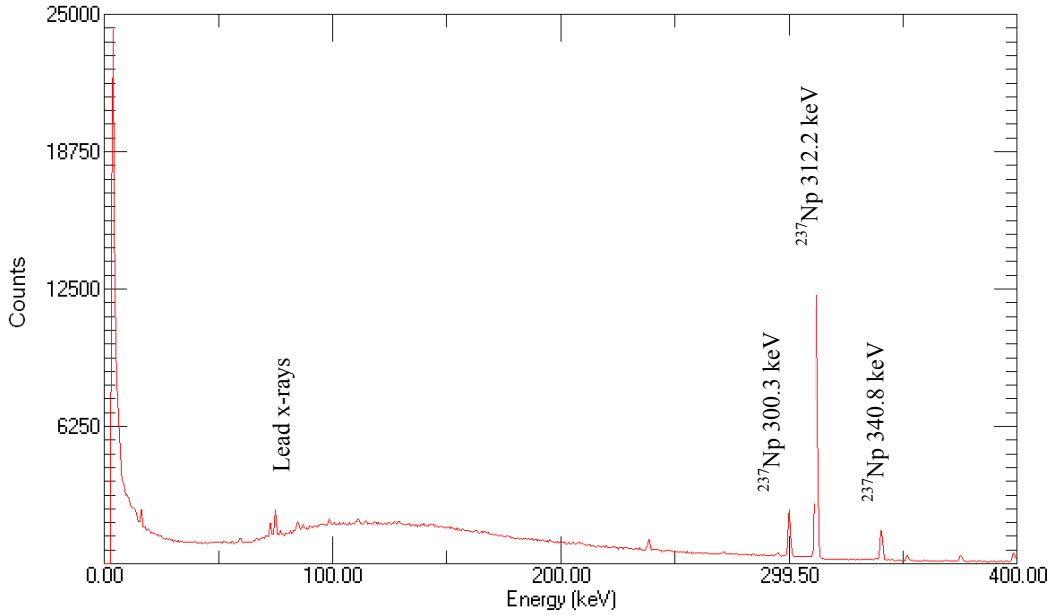


**Figure 3. Radial spectrum acquired from 50 inches.**

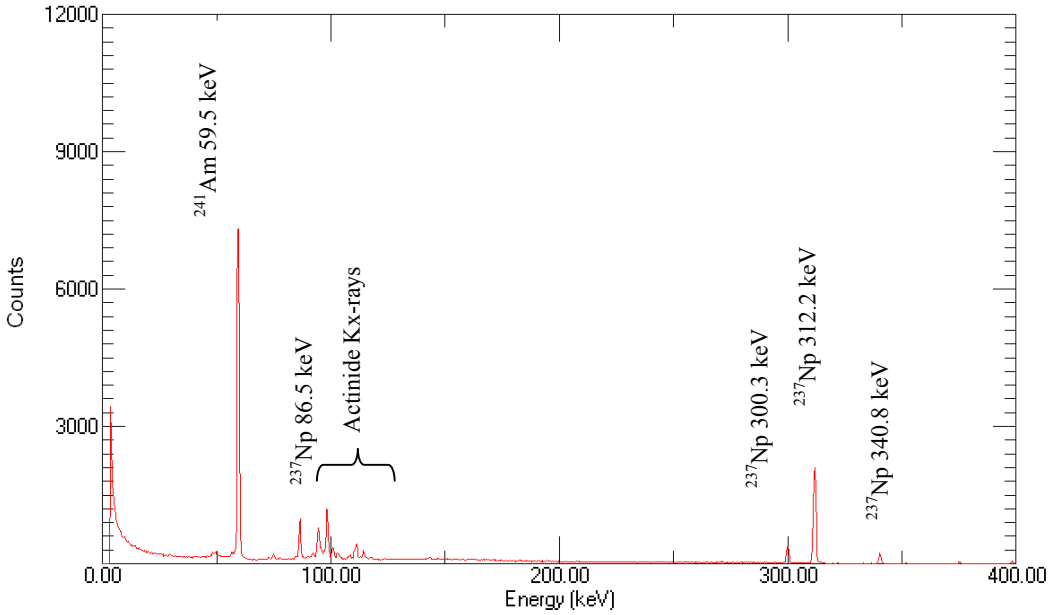


**Figure 4. Axial spectrum acquired from 36 inches.**

The 12-inch point source calibration curve for the 20% detector is shown in Figure 5 and is modeled by equation (1).

$$Ln[Eff(E)] = -8.033 + 0.9844x + 0.1632x^2 + 0.0019x^3 - 0.2120x^4, \quad (1)$$

where γ-ray energy E is in units of keV, and x equals the unusual form of ln[445.4/E].

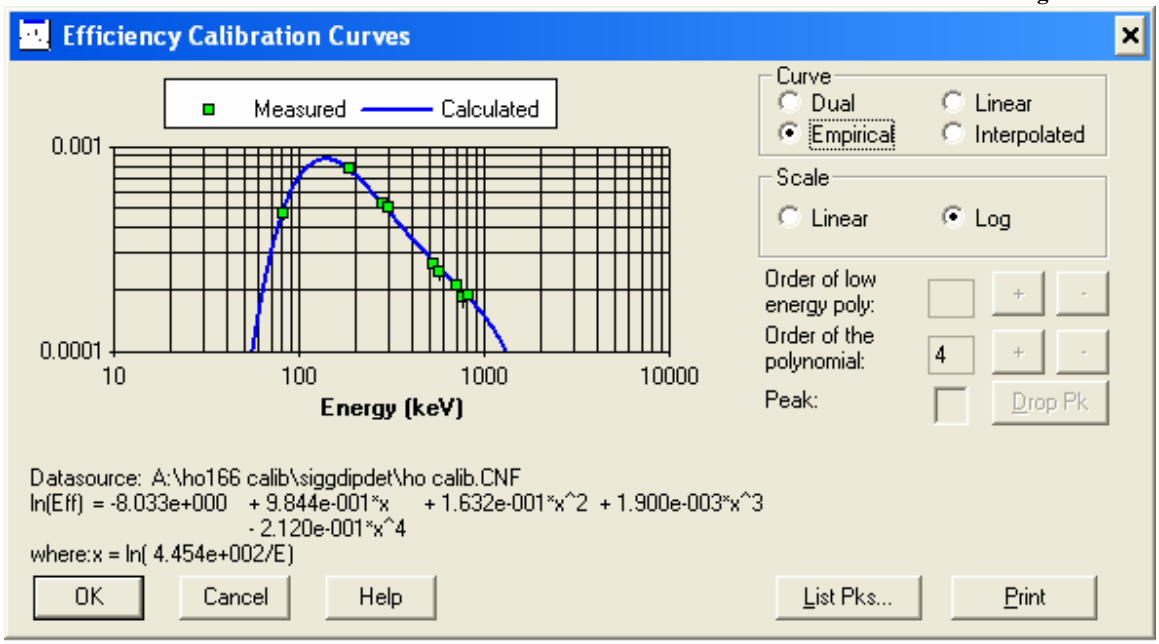


**Figure 5. The 12-inch point source efficiency calibration for the 20% detector used in these acquisitions.**

## CALCULATIONS AND RESULTS

### ISOTOPIC Analyses

The data were acquired in two distinct configurations and at two distinct acquisition distances in each configuration. This required three different models of the data using the ISOTOPIC code and provided an excellent test of the models. We deal first with the Am-241 Mossbauer activation source, which we modeled as a point source, and we then deal with the Np-237 contamination, which we modeled as an annular source of approximately null thickness.

Am-241 Point Source

The Mossbauer instrument was known to contain an Am-241 activation source inside as described in the **Experimental** section. Viewing this source from the side of the instrument we observed no 60-keV γ-rays, and this was interpreted as the 0.2-inch stainless steel outer shell providing infinite shielding of these low-energy photons. Our ISOTOPIC calculations indicated a total absorption factor of 6.12 for this γ-ray, and this would not be adequate to completely shield a source of near 5mCi. Thus it is apparent either sample self-absorption or some additional shielding was "hiding" this activation source.

The Pb x-ray doublets 73- and 75-keV and at 85-and 87-keV clearly demonstrate the existence of Pb shielding. However the GADRAS fit of the low energy continuum was unable to simultaneously fit the Pb K x-rays, a shielded 60-keV γ-ray from Am-241, and a shielded 86-keV γ-ray from Np-237. ISOTOPIC was unable to simultaneously fit the Pb x-rays, the Np-237 86-keV γ-ray, and the Pa-233 γ-rays with a consistent solution of Np-237 content. Of course the Pb x-rays and the Np-237 86-keV groups overlap considerably, and this makes fitting the low energy region and continuum very difficult. The solution was to assume an inner Am-241 point source shielded by Pb and steel and a separate outer, annular Np-237 source shielded only by 0.2-inches of steel.

Modeling the Am-241 source as a point source with an unknown lead shield in the two axial configuration acquisitions and completely disregarding the Np-237 yielded very good agreement between the two analysis codes and between the two acquisition distances. The Am-241 content was calculated by ISOTOPIC with equation (2)

$$\text{Activity } {}^{241}\text{Am} = (\text{cps})(Cf_T)(\text{geometry})/[\text{efficiency}(60,\ 12'')][\text{branch}], \qquad (2)$$

where $Cf_T$ comes from the ISOTOPIC calculation of sample and matrix absorption. Since the Am-241 source is able to shine through the whole in the bottom of the Mossbauer instrument, the only absorption correction is that for 77 inches of air (where we added five inches to the standoff distance to account for the distance to the Am-241 source). $Cf_T(\text{air}) = 1.039$. The geometry factor relates the conversion of a point source at 12 inches to the actual acquisition distance. For a point source configuration, this geometry correction is equal to $(d/12)^2$. The two terms in the denominator are the 12-inch detection efficiency and the 60-keV branch in the decay of Am-241.

For acquisition *axial 72,* ISOTOPIC determined an activity of

$$\text{Activity } {}^{241}\text{Am} = (84.30)(1.039)(41.17)/[0.000144][0.359] = 6.975\text{x}10^7 \text{ dps}. \qquad (3)$$

Np-237 Axial View

We modeled the two axial views of the Np-237 contamination as if the detector were viewing a cylindrical ring of height six inches and radius nine inches. The Np-237 is assumed to coat the inside of the ring in a mass-less residue so that there is no matrix (sample) self-absorption. In the axial view the detector views the ring up its center axis. (In fact the ISOTOPIC program forced us to substitute an eight inch square base for the 9 inch diameter ring.) Np-237/Pa-233 photons must pass through the 0.1-inch steel base to reach the detector. The Np-237/Pa-233 activity is determined by ISOTOPIC using equation (4).

$$\text{Activity } {}^{233}\text{Pa} = (\text{cps})(Cf_T)(\text{geometry})/[\text{efficiency}(312,\ 12'')][\text{branch}], \qquad (4)$$

where $Cf_T(\text{steel}) = 1.220$, $Cf_T(\text{air}) = 1.024$. The geometry correction to convert a 12-inch point source to a nine inch ring of height six inches at a standoff distance of 72 inches is 40.43. The 12-point source efficiency is 0.000469, and the 312-keV branch is 0.36.

Activity $^{233}$Pa = (30.18)(1.249)(40.43)/[0.000469][0.36] = $8.535 \times 10^6$ dps. (5)

Note a purely point source geometry correction factor would be simply $(72/12)^2 = 36$. Because the Np-237/Pa-233 activity is distributed on a cylinder of diameter 9 inches, ISOTOPIC has calculated an additional geometry factor of 1.123 to yield a net geometry factor of 40.43.

The overall geometry factor calculated by ISOTOPIC at a 36-inch standoff axial view is 11.00. The simple point source correction would be $(36/12)^2 = 9$, so the extended-to-point source geometry correction is 11.00/9.00 = 1.222. It is intuitively obvious that the extended-to-point correction should grow larger as the detector standoff is reduced.

To perform the extended-to-point source correction ISOTOPIC evaluates the surface area of the cylinder in the field of view of the detector viewing up the center axis of the cylinder. To obtain the geometry correction ISOTOPIC calculates the flux of photons leaving the surface of the cylinder in units of photons/inch$^2$ passing through the detector at a standoff distance of 36 inches and 72 inches. It compares that flux to that of a point source passing through the detector at a standoff distance of 12 inches.

Observing Figure 6, we see that the differential flux passing through the detector at a standoff distance 36 is defined by

$$\Phi(A) = S_{area}/4\pi\int_r\int_\phi dA/r^2 = S_{area}/4\pi\int_r\int_\phi dr R d\phi/r^2, \quad (6)$$

where R is the radius of the cylindrical instrument, 4.5 inches in this case. From Figure 6, we note that

$$r = R\csc\theta, \quad (7)$$

and $$dr = -\csc\theta \cot\theta \, d\theta. \quad (8)$$

$S_{area}$ is the photon emission rate in units of events/cm$^2$sec. Equation (6) expands to

$$\Phi(A) = S_{area}/4\pi\int_\theta\int_\phi -R\csc\theta \cot\theta \, d\theta \, R d\phi/R^2\csc^2\theta , \quad (6)$$

where we have transformed the sum over r to the sum over θ. From Figure 6 we see that the limits of θ are

$$\theta_1 = \text{Arctan}(4.5/36) = 7.125 \text{ deg to} \quad (9)$$

$$\theta_2 = \text{Arctan}(4.5/42) = 6.116 \text{ deg},$$

and the limits of ϕ are of course $0 - 2\pi$.

Equation (6) elegantly reduces to

$$\Phi(A) = -S_{area}/4\pi\int_\theta\int_\phi \cos\theta \, d\theta d\phi. \qquad (6)$$

$$= -S_{area}/4\pi\int_\phi[\sin(6.116) - \sin(7.125)]d\phi = 0.008746S_{area}.$$

Note we are comparing the flux from an extended area source with that from a point calibration source at 12 inches. Since the point source has been spread over a cylindrical area of $2{\cdot}4.5\pi(6) = 54\pi$ in$^2$, the equivalent point source flux for the 36-inch standoff cylindrical view is $0.008746/54\pi = 0.000051557S_{pt}$. The 12-in point source standoff flux is $S_{pt}/4\pi(12)^2 = 0.0005526S_{pt}$, for a total geometry correction of 10.72, in good agreement with that calculated above by ISOTOPIC - the difference being attributed to use of a square base in ISOTOPIC instead of a cylindrical base.

We can perform the same calculation with the 72-inch standoff. The calculus is identical with the limits of θ being Arctan(4.5/72) = 3.576 and Arctan(4.5/78) = 3.302. The resulting flux becomes $0.002387S_{area} = 0.00001407S_{pt}$ and yields a geometry correction of 39.27.

Both of the axial ISOTOPIC calculations and the exact calculus solutions yield measured values far larger than the radial or GADRAS solutions. We attribute this difference to the Np-237 residue likely occurring also on the 4.5-inch disk that forms the bottom plate of the instrument. We model that distribution in Figure 7, where the flux reaching the detector from a disk source is

$$\Phi(A) = S_{disk}/4\pi\int_z\int_\phi dA/r^2 = S_{disk}/4\pi\int_z\int_\phi z d\phi dz/r^2. \qquad (10)$$

Since the source is assumed uniform, and independent of z and r, integrating over $0 - 2\pi$ and substituting for $r^2 = x^2 + z^2$ yields

$$\Phi(A) = S_{disk}/2\int_z z dz/r^2 = S_{disk}/2\int_z z dz/(x^2 + z^2). \qquad (11)$$

Differentiating implicitly shows

$$2rdr = 2zdz, \qquad (12)$$

so that rdr = zdz, and

$$\Phi(A) = S_{disk}/2\int_r rdr/r^2. \qquad (13)$$

Substituting $u = r^2$, we have $1/2du/u$ inside the integral or

$$\Phi(A) = S_{disk}/4\int_u du/u = S_{disk}/4[\ln u], \qquad (14)$$

where u is evaluated from $x^2$ to $(x^2 + R^2)$. Then

$$\Phi(A) = [S_{disk}/4][\ln(x^2 + R^2) - \ln(x^2) \quad (15)$$

$$= [S_{disk}/4][\ln\{(x^2 + R^2)/x^2\}$$

$$= [S_{disk}/4][\ln(1 + R^2/x^2)].$$

For R = 4.5, and x = 36 we obtain

$$\Phi(A) = [S_{disk}/4][\ln(1.015625)] = 0.003876S_{disk}. \quad (15)$$

$S_{disk}$ is the equivalent point source spread over the area of the 4.5inch disk. So $S_{disk} = S_{pt}/\pi R^2 = S_{pt}/20.25\pi$, and $\Phi(A) = 0.00006093S_{pt}$. And the geometry correction for the detector's view of the disk source at 36 inches is 9.07. We also perform this geometry correction for the disk with a standoff distance of 72 inches. In this case

$$\Phi(A) = [S_{disk}/4][\ln(1.003906)] = 0.0009747S_{disk}, \quad (16)$$

and the geometry factor is 36.07.

With two disparate geometry factors, the photons from the disk are reaching the detector with slightly greater probablility than those from the upright cylinder. We need to remodel the ISOTOPIC calculation with this consideration. But first it is necessary to remodel the photon absorption of the disk photons.

Note in Figure 6 the photons from the cylinder that are passing through the thickness of steel of a = 0.1 inch must actually pass a thickness asecθ, so that the effective thickness is slightly larger than a. (This is actually more easily observed in Figure 7). Instead of modeling the absorption ($e^{-\mu a \sec\theta}$), which would be a complex problem with no exact solution ($\Phi(A) = S_{disk}/4\pi\int_r\int_\phi e^{-\mu a \sec\theta} dr R d\phi/r^2$), we choose to simply calculate an average thickness over all angels θ and to compare with the absorption over a thickness of steel a. That is, $e^{-\mu a \sec\theta}$ is approximately a constant over the angles 6.116 deg to 7.125 deg, so we have separated the absorption function from the geometry function. An exact solution can be modeled using an excel spreadsheet, and we have preformed that modeling in Appendix A. The results in A demonstrate that separating the two functions for the axial cylindrical acquisition agrees very closely to the non-separated model.

For the right cylinder, the average thickness through which the photons must pass to reach the detector is determined by

$$t_{ave} = \int_\theta a\sec\theta \, d\theta / \int_\theta \theta \, d\theta = a[\ln(\sec\theta + \tan\theta)]/\theta, \quad (16)$$

where both the numerator and denominator are evaluated separately at $\theta_1$ and $\theta_2$. That is, the numerator yields

$$a[\ln(1.005724 + 0.107152) - \ln(1.007782 + 0.125000)] = a[0.106948-0.124676]. \quad (17)$$

And the denominator yields (where we now are obliged to use units of radians instead of degrees)

$$0.106744 - 0.124355 = \quad -0.017611.$$

Finally,

$$t_{ave} = -0.017728a/-0.017611 = 1.006644a. \quad (16)$$

Note this yields an average absorption of ($e^{-1.006644\mu a}$), while the absorption evaluated at the two extremes of θ would be ($e^{-1.005724\mu a}$) and ($e^{-1.007782\mu a}$). Substituting $\mu a = 0.0818$,[6] we obtain an average transmission correction of 312-keV γ-rays of 1.08588, while the transmission correction at the two extremes of $\theta_1$ and $\theta_2$ are 1.08574 and 1.08593 respectively. Using the thickness a = 0.1 inch alone would have yielded a transmission correction of 1.08254. Clearly complicating the integral ($\Phi(A) = S_{cyl}/4\pi\int_r\int_\phi e^{-\mu a \sec\theta} dR d\phi/r^2$) would not be worth the added effort. For the acquisition distance of 72 inches our average thickness changes to 1.001798a, and the transmission correction of the 312-keV γ-ray is 1.08540.

Applying the same calculus to determine the average thickness in the disk configuration, yields limits for $\theta_1$ and $\theta_2$ of 0 to 7.125 deg for the 36-inch acquisition and of 0 to 3.576 deg for the 72-inch acquisition. The average thickness observed in the 36-inch disk acquisition is 1.002587a and in the 72-inch acquisition is 1.00065a. And these yield transmission correction factors of 1.08546 and 1.08530.

Np-237 Radial View

We modeled the two radials views of the Np-237 contamination as if the detector were viewing a cylindrical ring of height six inches and radius nine inches from the side of the cylinder. The Np-237 is once again assumed to coat the inside of the ring in a mass-less residue so that there is no matrix (sample) self-absorption. In this radial view the Np-237/Pa-233 photons must pass through the 0.2-inch steel side of the instrument to reach the detector. The Np-237/Pa-233 activity using the 50-inch standoff is determined by ISOTOPIC using equation (6).

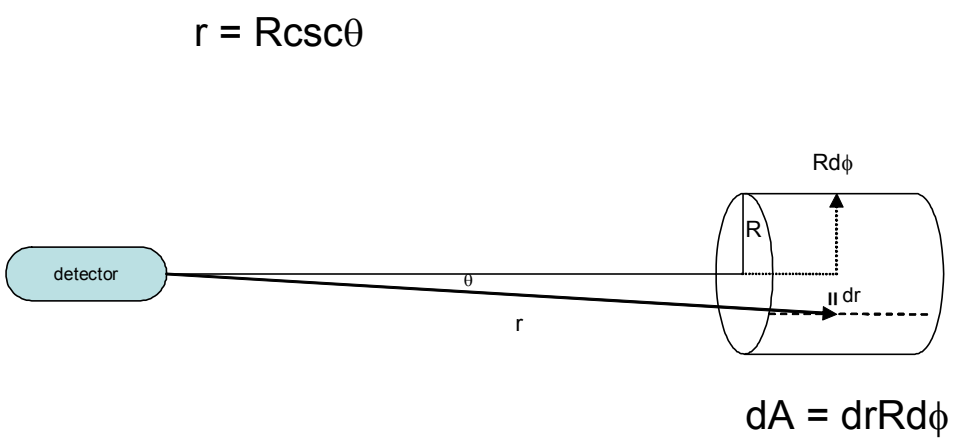


**Figure 6. Schematic view of cylindrical acquisition configuration showing r(θ), dr and dA.**

Activity $^{233}$Pa = (15.64)(1.512)(21.39)/[0.000469][0.36] = 2.995x10$^6$ dps, (6)

where $Cf_T$ (steel) = 1.488, $Cf_T$(air)= 1.016. The geometry correction to convert a 12-inch point source to a radial view of a nine inch ring of height six inches at a standoff distance of 50 inches is 21.39. The simple point source correction would be $(50/12)^2 = 17.36$, so the extended-to-point source geometry correction is 21.39/17.36 = 1.232.

We do not thoroughly solve the radial views with exact calculus, but rather describe the ISOTOPIC modeling. For the radial view obtained from 50 inches the distance x to the center of the cylinder of radius R = 4.5 is 54.5 inches. Therefore the distance r to the segment of area dA is

$$r(h,\phi)^2 = x^2 + R^2 - 2xR\cos\phi + h^2 \quad (17)$$

$$= 2500 + 20.25 - 490.5\cos\phi + h^2,$$

where ϕ is the angle described in Figure 8, and h is the height above or below the center of the cylinder. The measured flux independent of absorption by the 0.2 inch steel shell is then

$$\Phi(A) = S_{area}/4\pi\int_h\int_\phi dA/r^2 = S_{area}/4\pi\int_r\int_\phi dhRd\phi/r^2 \quad (18)$$

$$= S_{area}/4\pi\int_h\int_\phi dhRd\phi/(2500 + 20.25 - 490.5\cos\phi + h^2).$$

Transmission through the steel shell is $e^{-0.2\mu f(\phi)}$, where $f(\phi)$ varies as cosh(u); and u = 0 at $\phi = 0$ and u = R/x at $\phi = \pi/2$. This does not consider the effect of h on the transmission. In general

$$\Phi(A) = S_{area}/4\pi\int_r\int_\phi e^{-0.2\mu\cosh(u)}dhRd\phi/(2500 + 20.25 - 490.5\cos\phi + h^2), \qquad (19)$$

where $u = R\sin(\phi)/x$. This is an extremely complex integral that the code ISOTOPIC has modeled by summing over dh's and Rdϕ's. For a single arbitrary element r(-2.9, 1.2 rad), dh = 0.2, and dϕ = 0.2 rad we obtain

$$\Phi(A) = S_{area}\{e^{-0.2\mu\cosh(0.07759)}(0.2)(0.9)/(2520.25 - 177.74 + 9)\}/4\pi. \qquad (19)$$

$$= S_{area}\{e^{-0.1639)}(0.18)/(2351.51)\}/4\pi = 5.171\text{x}10^{-6}S_{area}.$$

$$= 3.048\text{x}10^{-8}S_{pt}.$$

Here we accept the sum modeled by ISOTOPIC, which yielded a total geometry correction of 21.39 relative to the 12 inch point source calibration and a total absorption correction of 1.488 for the 312-keV γ-ray. For the 25-inch radial acquisition the cosh(u) correction μa gets as large as 1.0117, and ISOTOPIC determined a total geometry correction of 6.33 and a transmission correction of 1.488 again. We discuss this exact agreement for transmission correction at two acquisition distances further below.

The results for each measured Am-241 and Np-237/Pa-233 contents are listed in Table 2. The GADRAS best fits are also included in Table 2. The GADRAS fit to spectrum *Radial 50* is shown in Figure 9 and to spectrum *Axial 36* is shown in Figure 10.

**Table 2. Compiled results from ISOTOPIC and GADRAS models.**

| | ISOTOPIC | | | GADRAS | |
|---|---|---|---|---|---|
| **Acquisition** | **Am-241 (μCi)** | **Np-237 (μCi) 312 keV** | **Np-237 (μCi) 300 keV** | **Am-241 (μCi)** | **Np-237 (μCi)** |
| ***Axial 36*** | **1670±65** | **217±18** | **210±18** | **2000** | **106** |
| ***Axial 72*** | **1697±66** | **227±10** | **222±6** | **1800** | **110** |
| ***Radial 25*** | **Not observable** | **59±4** | **56±4** | **Not observable** | **85** |
| ***Radial 50*** | **Not observable** | **76±3** | **74±5** | **Not observable** | **103** |

Using the 312-keV Np-237/Pa-233 values only from ISOTOPIC (so that we do not overweight the ISOTOPIC determinations) we determine an observed Am-241 content of 1791±150 μCi, and a measured Np-237 content of 122±63 μCi. We believe the Np-237 results represent fairly good agreement between two techniques of analyses and two distinct acquisition configurations. However we can improve those agreements as we do in the **Discussion** section.

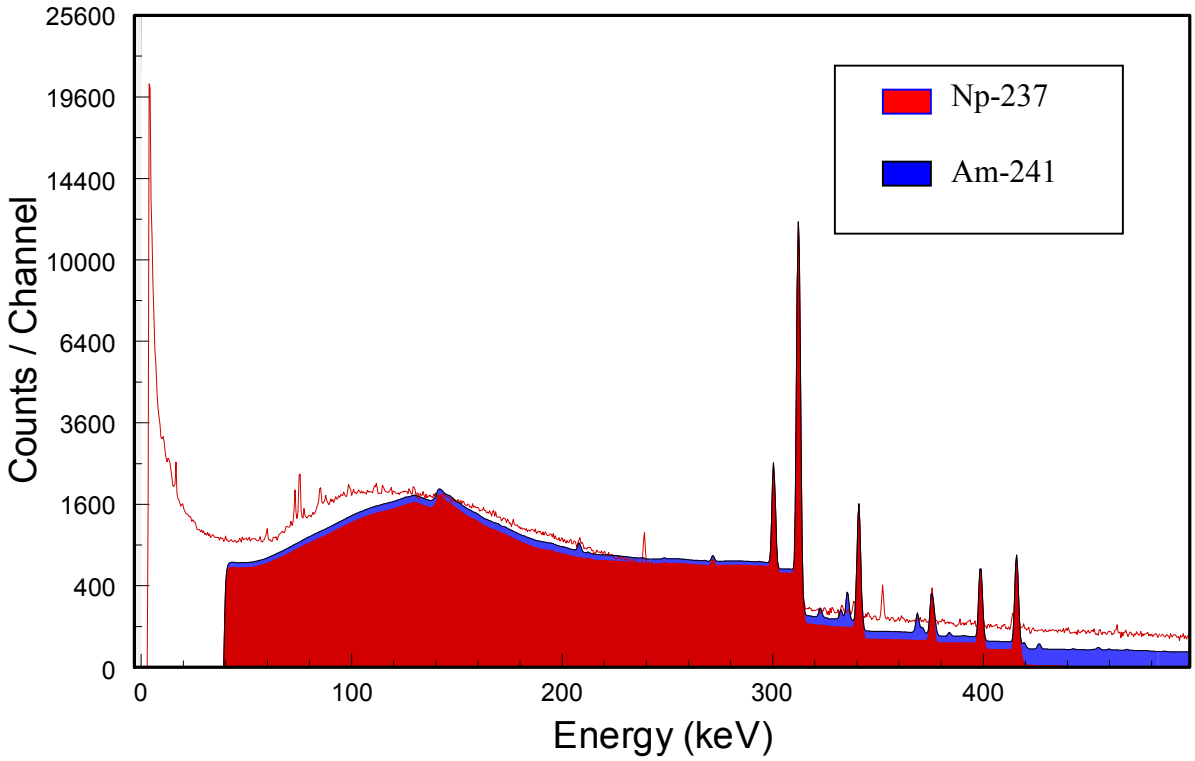


**Figure 9. GADRAS full-spectrum fit to spectrum *Radial 50*. The red shading indicates the Np-237/Pa-233 contribution, and the blue shading indicates the Am-241 contribution.**

The agreement by ISOTOPIC between the two T correction values to four significant figures for the two axial views would seem to indicate some deficiency in that calculation, as we observed in the axial acquisitions. That is, by exact calculus they should not agree so closely at the two differing acquisition distances. However we believe the largest "deficiency" is not including the contributions from the disk base. So it is important to attempt to model that using an excel spreadsheet and carefully depicting each $d\Phi(A)/dA$ segment for the disk.

We note also that GADRAS does not fit the continuum in the radial spectrum of Figure 9 and has not accounted for fluorescence of the Pb x-rays at 94 and 99 keV in the axial spectrum of Figure 10. Neither of these two issues significantly affects the Np-237 content determined by GADRAS. The photopeaks from that species are all fit extremely well in both spectra.

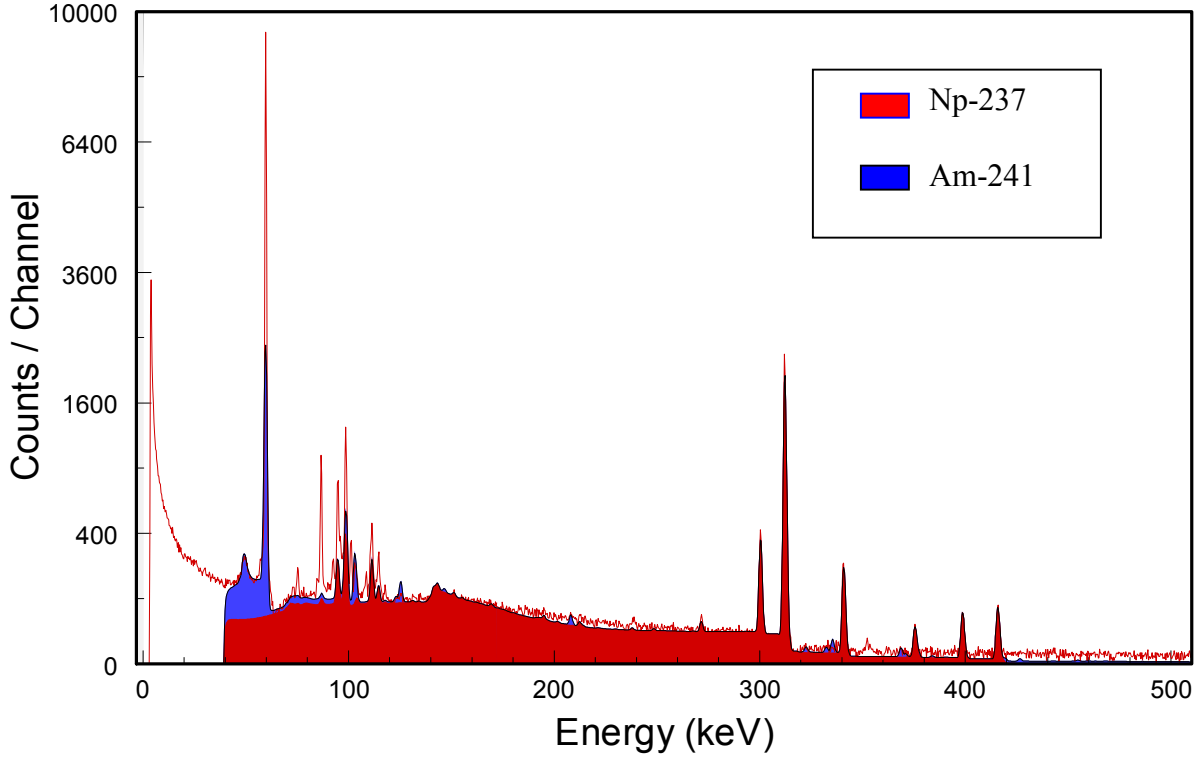


**Figure 10. GADRAS full-spectrum fit to spectrum *Axial 36*. The red shading indicates the Np-237/Pa-233 contribution, and the blue shading indicates the Am-241 contribution.**

**Discussion**

Remodeling the Axial Acquisitions with Cylindrical Plus Disk Field of View

We note in Table 2 that for the ISOTOPIC modeling the radial and axial results disagree significantly. We believe the difference is largely because neither model includes contributions from the base to the acquired spectra. That is, both models include only contributions to the spectra from the cylinder. In the axial views, the disk base is closer to the detector than the cylinder, and so the detector views photons from the base with a higher efficiency than those from the cylinder. Thus modeling only the cylinder yields a positive bias in the results. For the radial views the opposite is true and the results are negatively biased. We have attempted to add the two contributions and to reanalyze.

In order to remodel we have assumed that the Np-237 contamination is equally distributed per unit area on to the cylinder and base. Since the base has a total surface area of $A(\text{base}) = \pi R^2 = 20.25\pi$, and the cylinder has a surface area of $A(\text{cylinder}) = 2\pi Rh = 54\pi$, the cylinder has 72.7% of the Np-237 activity, and the base has 27.3%. We remodeled with that assumption and with the slightly larger photon absorption in the cylindrical case. We used the absorption factors determined from the average thicknesses of equation (16). These factors are all near 1.08, while the ISOTOPIC factors are near 1.22. Results are displayed in Table 3 where we assign uncertainties equal to the same percentages as the ISOTOPIC model in Table 2.

The summed cylinder plus disk model yields measured activity A of (for the 36 inch axial acquisition).

$$A(36\ \text{axial}) = \frac{(0.727)(cps)(Cf_{abs\ cyl})(Cf_{geo\ cyl})}{(eff)(branch)} + \frac{(0.273)(cps)(Cf_{abs\ disk})(Cf_{geo\ disk})}{(eff)(branch)}. \quad (18)$$

$$= \frac{(0.727)(106.71)(1.08314)(10.72)}{(0.000469)(0.36)} + \frac{(0.273)(106.71)(1.08275)(9.07).}{(0.000469)(0.36)}$$

$$= 7.030\text{x}10^{6}\ \text{dps} = 190\mu\text{Ci}.$$

Our correction is at least in the right direction. We do the same in the radial acquisitions after modeling the disk acquisitions taken from the side looking over the disk using ISOTOPIC.

Remodeling the Radial Acquisitions with Cylindrical Plus Disk Field of View

For the view looking over the disk, the element of flux is a function once again of r and $\phi$ with h = -3 always as shown in Figure 11.

$$\Phi(A) = S_{disk}/4\pi\int_z\int_\phi dA/r^2 = S_{disk}/4\pi\int_z\int_\phi drRd\phi/r^2 \quad (20)$$

$$= S_{disk}/4\pi\int_z\int_\phi dzzd\phi/r^2 = S_{disk}/4\pi\int_z\int_\phi zdzd\phi/(x^2 + z^2 - 2xzcos\phi + h^2).$$

For the x = 50 inch acquisition this yields

$$\Phi(A) = S_{disk}/4\pi\int_z\int_\phi zdzd\phi/(50^2 + z^2 - 100zcos\phi + 3^2).$$

And including the absorption over $\phi$

$$\Phi(z,\phi) = S_{disk}/4\pi\int_z\int_\phi zdzd\phi e^{-0.2\mu cosh(u)}/(2509 + z^2 - 100zcos\phi). \quad (21)$$

In this case h is always equal to -3, and we believe the contribution of that pathway through the 0.2-inch steel must be included. This increases the thickness of 0.2 to $0.2sec\theta$ as in the axial acquisitions. Theta is a complicated function of z and $\phi$.

$$\theta = Arctan[\sqrt{(z^2 + 9 - 6zcos\phi)}/r], \quad (22)$$

but is always approximately equal to 4 deg. We insert that correction for $0.2\mu$ into (21).

$$\Phi(A) = S_{disk}/4\pi\int_z\int_\phi zdzd\phi e^{-0.2005\mu cosh(u)}/(2509 + z^2 - 100zcos\phi). \quad (21)$$

The element $\Phi(2.25,5.1)$ with dz = 0.1 and $d\phi$ = 0.2 rad is

$$\Phi(z,\phi) = S_{disk}/4\pi\int_z\int_\phi z dz d\phi e^{-0.2005\mu\cosh(u)}/(2509 + z^2 - 100z\cos\phi)\}. \quad (21)$$

$$= S_{disk}/4\pi\{2.25(0.1)(0.2)e^{-0.2005\mu\cosh(-0.03322)}/(2514.06 - 85.04).$$

$$= S_{disk}/4\pi\{0.0000157) = 1.251x10^{-6}S_{disk.}$$

$$= 1.967x10^{-8}S_{pt.}$$

The 2.06 version of ISOTOPIC is unable to model a detector viewing over a disk source, but it is able to model viewing over a rectangular source. We used that model with dimensions 8x8 to approximately model the disk. Another option is to simply use the ratios of the individual elements in equations (19) and (21) to represent the relative flux obtained from the radial acquisitions of a cylinder and horizontal disk. This is likely just as accurate as the overall assumptions we've used to distribute the total activity over the cylinder and disk.

Using the view over a square plane of 8" side and with the detector looking across the plane at a height of 3 inches, ISOTOPIC modeled a geometry correction factor of 21.05 relative to a 12-inch point source and an absorption correction factor of 1.512 from an acquisition distance of 50 inches. From 25 inches those values were modeled as $Cf_{geo\ plan}$ = 6.17, and $Cf_{abs\ plan}$ = 1.504.

We use those values and distribute the observed activity in the radial acquisitions in the same manner as above in the axial acquisitions.

$$A(50\ radial) = \frac{(0.727)(cps)(Cf_{abs\ cyl})(Cf_{geo\ cyl})}{(eff)(branch)} + \frac{(0.273)(cps)(Cf_{abs\ plan})(Cf_{geo\ plan})}{(eff)(branch)}. \quad (23)$$

$$= \frac{(0.727)(15.64)(1.488)(21.39)}{(0.000469)(0.36)} + \frac{(0.273)(15.64)(1.512)(21.05)}{(0.000469)(0.36)}$$

$$= 2.948x10^6\ dps = 79.7\mu Ci$$

for the 50 inch acquisition. For the 25 inch acquisition our sum is 61.9μCi. The corrected values in Table 3 are once again at least in the right direction.

As a check, we note the ratio of the two terms in (23) is 0.376, which is equivalent to stating that even though we assume 27% of the activity is one the disk bottom, ISOTOPIC calculates that the bottom makes a 38% corrected contribution to the calculated value. Using the ratios for the element of flux calculated in (19) and (21) we would determine that the disk bottom makes a 58% contribution to the calculated value. This would bring the values in Table 3 up further still.

**Table 3. Summed model where the results in column 2 represent exact calculus and contributions from both the base a cylinder in the axial acquisitions.**

| | Summed Model | GADRAS |
|---|---|---|
| **Acquisition** | **Np-237 (μCi) 312 keV** | **Np-237 (μCi)** |
| ***Axial 36*** | **190±16** | **106** |
| ***Axial 72*** | **179±8** | **110** |
| ***Radial 25*** | **61.9±4** | **85** |
| ***Radial 50*** | **79.7±3** | **103** |

Applying the values of Table 3 yields a reported Np-237 content of 114±46 μCi. The detailed analysis has reduced the overall uncertainty significantly compared to the results of Table 2

## CONCLUSION

Using the ISOTOPIC analysis code, the GADRAS analysis code, and exact calculus where possible, we have performed analysis of six γ-ray acquisitions to compare Am-241 and Np-237 residual contamination in a Savannah River National Laboratory Mossbauer activation spectroscopy instrument. Residual Np-237/Pa-233 content was observed and analyzed in both radial and axial views of a cylinder plus base configuration with all three analytical tools.

Using exact calculus we have tested the geometry corrections and transmission corrections of both systems. We have also demonstrated the modeling of differential elements of flux for both the cylinder and disk base for both views. We have modeled the absorption correction of the axial views with simple trigonometry combined with exact calculus to separate a complicated integral into to integrals that can be solved exactly. We have modeled the absorption correction of the radial views with the hyperbolic cosine function combined with exact differential element modeling to approximately solve the exact calculus. Both of these approaches agree well with the ISOTOPIC and GADRAS analyses.

From our combined analyses we have been able to bring the axial and radial determinations by ISOTOPIC into closer agreement with those determined by GADRAS. Since the GADRAS technique of fitting uses the entire photopeak plus Compton continuum of each spectrum, it should be expected to be the more powerful analysis technique if it is used properly. The results of this paper demonstrate that capability, as the axial and radial views of the instrument analyzed here are in significantly better agreement than those two views analyzed by the uncorrected ISOTOPIC technique.

**Figure 7. Schematic view of an axial acquisition of the disk bottom.**

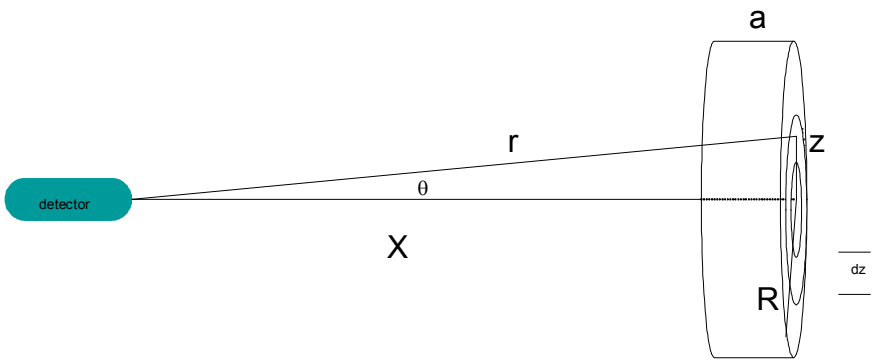

**Figure 8. Schematic view of a radial acquisition of a cylinder.**

$\phi$ is the angle formed by the projection of R from the center of the cylinder to it's intersection with r at the surface.

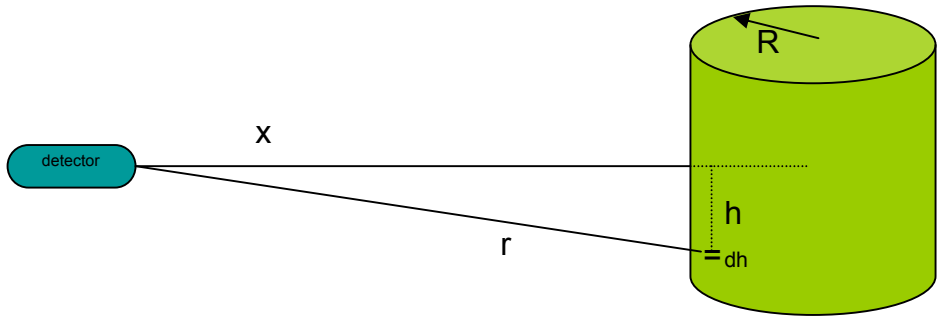

**Figure 11. Acquisition described in text where the detector views over a disk.**

$\phi$ is the angle formed by the projection of z up (z') so that it intersects with x + R.

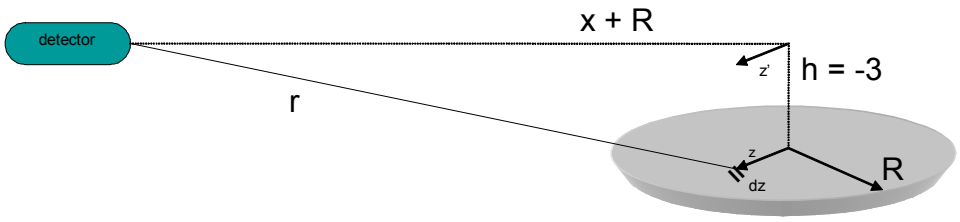

## REFERENCES

1. Ametek Ortec Gamma-ray analysis computer code Isotopic version 2.0.6.

2. R. A. Dewberry, V. R. Casella, R. A. Sigg, S. R. Salaymeh, F. S. Moore, and D. J. Pak "Holdup Measurements for three Visual Examination and TRU Remediation Glovebox Facilities at the Savannah River Site", **Journal of Radioanalytical and Nuclear Chemistry**, Vol. 275, No.3 (2008), December 2008.

3. R. A. Dewberry, V. R. Casella, R.A. Sigg, and N. N. Bhatt, "Benchmarking Ortec Isotopic Measurements and Calculations", **J. Radioanalytical and Nuclear Chemistry**, Vol 281, No. 3 (2009) 313.

4. Gamma Detector Response Analysis Software (GADRAS). Mitchell, Dean, GADRAS Gamma Analysis Software, Version 15.1.2, Sandia National Labs.

5. R. A. Dewberry, R. A. Sigg, and S. R. Salaymeh, "Gamma-Pulse-Height Evaluation of a USA Savannah River Site Burial Ground Special Configuration Waste Item", **J. Radioanalytical and Nuclear Chemistry**, Vol 283, No. 1, (2009), Jan. 2010.

6. J. R. LaMarsh, Introduction to Nuclear Engineering, 2nd Ed., (Addison-Wesley, Reading MA, 1983).

| $\Phi(A) = S_{area}/4\pi r^2$ line source (does not include sum over angle $\phi$) | | | | | | | | | | | | | |
|---|---|---|---|---|---|---|---|---|---|---|---|---|---|
| **h** | **r** | **θ(deg)** | **θ(rad)** | **csc(θ)** | **r(θ)** | **flux(dA)** | **dh** | **Summed flux** | **Flux(dA) t corrected** | **Summed flux t corrected** | | | |
| 36.3330 | 36.6106 | 7.0604 | 0.1232 | 8.1357 | 36.6106 | 5.9371E-05 | 0.6667 | | 5.8891E-05 | | | | |
| 37.0000 | 37.2726 | 6.9343 | 0.1210 | 8.2828 | 37.2726 | 5.7281E-05 | 0.6667 | | 5.6818E-05 | | | | |
| 37.6670 | 37.9349 | 6.8127 | 0.1189 | 8.4300 | 37.9349 | 5.5299E-05 | 0.6667 | | 5.4851E-05 | | | | |
| 38.3330 | 38.5962 | 6.6954 | 0.1169 | 8.5769 | 38.5962 | 5.3420E-05 | 0.6667 | | 5.2987E-05 | | | | |
| 39.0000 | 39.2588 | 6.5819 | 0.1149 | 8.7242 | 39.2588 | 5.1632E-05 | 0.6667 | | 5.1214E-05 | | | | |
| 39.6670 | 39.9214 | 6.4722 | 0.1130 | 8.8714 | 39.9214 | 4.9932E-05 | 0.6667 | | 4.9528E-05 | | | | |
| 40.3330 | 40.5833 | 6.3662 | 0.1111 | 9.0185 | 40.5833 | 4.8317E-05 | 0.6667 | | 4.7925E-05 | | | | |
| 41.0000 | 41.2462 | 6.2635 | 0.1093 | 9.1658 | 41.2462 | 4.6776E-05 | 0.6667 | | 4.6397E-05 | | | | |
| 41.6670 | 41.9093 | 6.1640 | 0.1076 | 9.3132 | 41.9093 | 4.5307E-05 | 0.6667 | 5.1926E-05 | 4.4940E-05 | **5.1506E-05** | **T(ave)=** | **1.006644** | 0.008234 |
| | | | | | | | | | **Sum uncorrected flux times Abs(ave)** | **5.1583E-05** | | | |

**Appendix. Matrix element sum of vertical line source to simulate integral including container absorption over an axial view of a cylindrical source.**